Supporting Online Material for

NADP regulates the yeast *GAL* induction system

P. Rajesh Kumar[1], Yao Yu[2], Rolf Sternglanz[2], Stephen Albert Johnston[3], Leemor Joshua-Tor[1*]

[1]Cold Spring Harbor Laboratory, 1 Bungtown Road, Cold Spring Harbor, NY 11724
[2]Department of Biochemistry and Cell Biology, Stony Brook University, Stony Brook, NY 11794-5215
[3]Center for Innovations in Medicine, Biodesign Institute, Arizona State University, PO Box 875901, Tempe, AZ 85287-5901
*To whom correspondence should be addressed: leemor@cshl.edu

SUPPORTING TEXT

Gal80p architecture

We utilized two super-repressor mutants of ScGal80p, Gal80p^{S2} and Gal80p^{S0} for crystallization experiments with two different peptides in various combinations to enhance our probability for obtaining crystals (see Materials and Methods). P21 is a 21 amino acid peptide that contains the conserved region of the C-terminal AD of Gal4p (aa 854-874). P20 is a peptide that was identified from a phage-display screen selected for Gal80p binding and was also shown to activate transcription (*1*). Gal80p^{S2}:P20 formed monoclinic crystals with 6 molecules in the asymmetric unit consisting of three independent dimers. Gal80^{S0}:P21 formed orthorhombic crystals with two molecules in the asymmetric unit forming a single dimer. Initially the structure of the monoclinic complex was determined using the MIR(AS) method (see Materials and Methods). A partial polyalanine model was built into this experimental density and was then used to phase the higher resolution orthorhombic crystal by molecular replacement. Side chains were built for the higher resolution structure and the more accurate model was transformed back to the monoclinic crystal structure. A structure based alignment performed using the DALI server (*2*) suggest that ScGal80p closely resembles the structure of glucose-fructose oxidoreductase (PDB code: 1OFG (*3*)) from *Zymomonas mobilis*, as does the KlGal80p structure (*4*).

The crystal structures of ScGal80p reveal a three-domain architecture with an N-terminal domain consisting of a classic Rossmann fold, and a C-terminal domain consisting of a large β-sheet that forms an extensive dimer interface with another monomer (Figure 2). A large cleft is apparent between these two domains. A smaller third domain is located between the N and C-terminal domains consisting of three small β -strands and an α-helix. The β sheets at the dimer interface are not parallel to each other but are arranged in a V shape (Fig. 1A). The two super-repressor mutations used in this study (Gal80^{S0} and Gal80^{S2}) are located on the large β-sheet but point toward the cleft rather than toward the dimer interface. The third super repressor mutation, Gal80^{S1}, is located in very close proximity but is on a disordered loop (see Fig S2).

Gal80p dimers form higher order oligomers

The three dimers in the monoclinic crystals form two tetramers – one between two of these dimers and a third between dimers related by crystallographic symmetry (Fig S3). The same type of tetrameric arrangement is also seen between crystallographically related dimers in the orthorhombic form. Gal4p binds its UAS$_{GAL}$ DNA binding site as a dimer (*5-7*) and therefore a dimeric structure of its repressor might be expected. Both *GAL1* and *GAL10* have four UAS$_{GAL}$ elements whereas *GAL2* and *GAL7* have two. *MEL1* and *GAL80*, on the other hand, have only one UAS$_{GAL}$. It has been postulated that Gal80p dimer-dimer interaction on adjacent Gal4p dimers could explain the synergistic tighter regulation of the *GAL1* and *GAL10* genes whereas the basic dimer regulates a low-level constitutive expression of the *GAL80* and *MEL1* genes (*8*). We propose that the tetrameric organization seen in our crystal structures represents the

dimer-dimer interaction of Gal80p associated with tighter control *in vivo*. The most notable utilization of dimer-dimer interactions between repressor proteins on adjacent sites for tight regulation is of course the case of λ repressor, where the interactions between dimers increase specificity and affinity to the DNA (*9*).

A dinucleotide between Gal80p and Gal4p

In the ScGal80p^{S2}:P20 structure, we identified electron density indicating an NAD dinucleotide bound to the cleft of the protein at the Rossmann fold as seen for other oxidoreductases, despite the fact that no dinucleotides were added to our purification or crystallization buffers at this point. We therefore decided to soak the ScGal80p^{S0}:P21 crystals, which diffracted to higher resolution, with NAD in order to replenish what might have been lost during purification. Not only did the density of this dinucleotide become even more apparent (greater than 4σ level and around 9σ for the phosphates) than in the unsoaked crystals (Fig. S4), but we were then able to locate a portion of the Gal4p AD peptide, which we were unable to observe previously, bound to the cleft in each monomer of Gal80p (Fig. S5). NAD appears to be nestled between Gal80p and P21 in the cleft of the protein. We observe the Gal4p peptide only in the NAD-soaked Gal80^{S0}:P21 crystals and not in the structure of ScGal80^{S2}. We have modeled a segment of the peptide consisting of 9 residues for one monomer and 5 residues for the other. Although the backbone electron density is clear, most side chains seem to be somewhat disordered and could not be unequivocally assigned. As a precaution, we omitted the modeled peptide and re-refined (Fig. S3). The density re-appeared at 3σ level, confirming the location of the peptide.

As mentioned in the main text, the crystal structure of KlGal80p did not show any bound dinucleotide (*4*). The authors argued that their structure suggests that NAD(P) could not bind based on a difference in the conformation of a short loop containing the dinucleotide binding motif in comparison with other NAD(P) bound oxidoreductases. However, this loop is in the same conformation in ScGal80p and binds the dinucleotide.

E122 and W123 instead of a lysine, form part of the conserved motif “EK(P/A)” found in other oxidoreductases. The third residue of this motif is usually found in a *cis*-conformation in the oxidoreductases and indeed A124 is in a *cis*-conformation at this position in this structure as well.

Several key interactions are made by ScGal80p and NAD (Fig. 1B). The side chains of Q151 and H213 hydrogen bond to N7 and O7 of the nicotinamide ring. W31 stacks on top of the nicotinamide ring. Other notable hydrogen bonds are from a carboxylate oxygen of E122 to the N7 atom of the nicotinamide and the main-chain carbonyl atom of W123 to the 2’-hydroxyl of the nicotinamide ribose. In addition, the amide of N26 hydrogen bonds to the adenine ribose.

Significance of the dimer interaction

The mutation in the dimeric interface, N230R, resulted in a phenotype with considerable expression in the uninduced state, though not to the same level as a *gal80*Δ strain. This indicates that Gal80p dimerization is important for Gal4p binding and therefore repression. The dimer interface is quite extensive, with a buried surface area of 4990

Å^2, however, and a single point mutation would probably not cause complete disruption of the dimer, and therefore not a complete loss of repression.

Materials and Methods

Protein Expression and purification

Wild type Gal80p (2-435) (wtGal80) was generated from S. cerevisiae genomic DNA using standard PCR protocols. The wild type Gal80p (wtGal80p) and the super-repressor point mutations ($Gal80^{S0}$ – G301R, $Gal80^{S1}$– G323R, $Gal80^{S2}$ – E351K) were cloned into pET28a using standard protocols, yielding a construct that expresses Gal80/$Gal80^{S0,S1,S2}$ with an N-terminal $(His)_6$-tag which can then be cleaved by the thrombin protease. wtGal80p and mutants were expressed in BL21(DE3)-RPIL *E. coli* cells grown to a OD600=0.9 at 30°C in a fermenter in LB media and induced with 0.25 mM IPTG and the protein expression allowed to proceed at 18°C for an additional 16hrs. The cells were suspended in buffer A (20mM Tris (pH8.0), 10mM imidazole, 0.5M NaCl, 10% glycerol) and sonicated in the presence of 0.1% Triton X-100 and 1mM PMSF. The cleared lysate was passed through a column containing Ni-NTA agarose (Qiagen) equilibrated with buffer A. The column was then extensively washed with buffer A to remove the contaminating *E. coli* proteins. At this stage buffer A was replaced by a large excess of buffer B (20mM Tris, 0.1M NaCl, 10% glycerol) to facilitate thrombin cleavage of the N-terminal His tag and subsequent purification. On-bead digestion with 100U of thrombin was carried out for 20hrs at 17°C and the tag-free protein was eluted. This protein was then purified using a 5ml pre-packed heparin column coupled to an ÄKTA Explorer purification system (GE Healthcare). The protein was subjected to a gradient of 0-2M NaCl in the presence of 20mM Tris (pH8.0), 1mM EDTA, 5mM DTT, 10% glycerol. Gal80 elutes between 0.5-0.7M NaCl. Fractions containing Gal80p were concentrated and subjected to size-exclusion chromatography

on a Superdex 200 (26/60) column and the protein elutes at a volume that corresponds to a dimer of Gal80p. The dimerization and homogeneity of Gal80p was confirmed by dynamic light scattering experiments performed at 4, 17 and 25°C respectively and judged to be greater than 95% homogeneous. SDS-PAGE confirmed the purity of Gal80p to be greater than 95%. Overall protein yield is approximately 40mg from 12L of cells. Following concentration and quantification the protein was aliquoted and stored in 20mN Tris (pH 8.0), 0.1 M NaCl, 1mM EDTA, 5mM DTT, 10% glycerol, at -70°C for further crystallization experiments.

Crystallization

Gal80p^{S2} was incubated with the peptide P20 (NH_2-YDQDMQNNTFDDLFWKEGHR-COOH) in a 1:2 molar ratio for at least 30 minutes prior to crystallization. Vapor diffusion using the hanging drop method was used. The drop consisted of the protein-peptide complex, 9% sucrose, 4% γ -butyrolactone and an equal volume of reservoir solution containing 0.1M CAPS (pH 10.1), 0.25 M NaCl, 20% PEG 8000, 0.2 M sodium formate, 50 mM DTT, and 4% γ-butyrolactone. Optimization using micro-seeding procedures improved crystals to a final size of 0.6 x 0.15 x 0.1 mm.

Gal80p^{S0} was incubated with P21 (NH_2-GMFNTTTMDDVYNYLFDDEDT-COOH) in a 1:2 molar ratio, at 17˚C, for 30 min. The drop consisted of equal volumes of the protein-peptide complex and the reservoir solution consisting of 0.1-0.2 M NaF, 20% (w/v) PEG 3350. Crystals appeared overnight and reached maximum size of 0.2 x 0.2 x 0.2mm in 3-5 days.

Data collection and phasing

Data to 2.85 Å were collected on Gal80p^{S2}:P20 crystals. Selenomethionine incorporated crystals diffracted to 3.5 Å but were not sufficient to completely phase 6 molecules in the asymmetric unit. For this purpose the crystals were gradually transferred to buffer solutions around neutral pH to facilitate soaking experiments. Crystals were soaked in a solution containing Ta_6Br_{14} (a kind gift from Dr. Zbignew Dauter's group) and ethylene glycol as the cryoprotectant. Data were collected at 1.2519 Å wavelength to 4 Å resolution at 19-ID, APS.

12 Tantalum cluster positions were readily identified and refined by SHELXD (*10*) using data between 20-5 Å. These sites were incorporated into AUTO-SHARP (*11*) and combined with the native and selenomethionine data sets and several Se sites were found. Further heavy atom detection and refinement in SHARP led to the identification of 40 Se positions, using data between 20-3.5 Å. The experimental electron density was further subjected to solvent-flattening and phase extension to 2.85 Å using SOLOMON (*12*). At this stage the electron density revealed secondary structure features, including the large sheet at the dimeric interface of Gal80p. A polyalanine model was built including 60% of the total residues with O (*13*). We then obtained a higher resolution data set for an orthorhombic crystal form of Gal80p^{S0}:P21 that diffracted to greater than 2.1 Å. Molecular replacement with the program Phaser (*14*) with the partial polyalanine model clearly identified the dimer in the asymmetric unit for this data set. Further rounds of model building and side-chain placement and refinement with REFMAC (*15*), gave a more complete model. The nearly complete model was then transformed back to the

monoclinic cell with the appropriate mutations for Gal80p^{S2} and further refined. During the initial stages of refinement, strict non-crystallographic symmetry (NCS) constraints were maintained and a gradual shift to lower-weight restraints were maintained until the end of refinement. Monomers A-D had more similarities and hence they were restrained into one NCS group and monomers E and F were restrained as a separate NCS group during later stages of refinement.

Orthorhombic crystals of the Gal80p^{S0}:P21 complex were soaked with β-NAD (Roche) to a final concentration of 5mM, for 2h, and gradually transferred to a mother liquor containing 25% ethylene glycol and 5mM NAD and frozen in liquid nitrogen. These crystals diffracted to 2.7 Å. A difference map, with the refined Gal80p^{S0}:P21 structure, showed clear electron density for the two NAD molecules in each Gal80p monomer at >4σ level. Additional elongated electron density greater than 3σ proximal to the nicotinamide group of the NAD was observed in both monomers (Fig. S5A). Two short peptides (9 residues for one monomer and 5 residues for the second monomer) were built into this electron density. The locations of these peptides were further verified by calculating an omit map, where the peptides were omitted and the rest of the coordinates randomly perturbed and subjected to refinement until convergence (Fig. S5B). Strict NCS constraints between the dimers was employed during initial stages of refinement and were gradually released.

Final models are missing the following protein residues:

Gal80p^{S0}-Gal4AD-NAD: Chain A: 1-12; 283-290; 308-311; 323-346; 380-387; 434.

Chain B: 1-14; 250-252; 283-289; 310-313; 323-343; 378-387.

Gal80p^{S0} : Chain A: 1-15; 283-290; 309-311; 323-344; 380-384.

Chain B: 1-15; 248-252; 283-289; 310-311; 325-346.

Gal80p^{S2} Chain A: 1-15, 326-348; 381-386.

Chain B: 1-14; 323-346; 381-386.

Chain C: 1-15; 326-347; 381-386.

Chain D: 1-15; 326-346; 380-386.

Chain E: 1-16; 326-347; 381-386; 433-434.

Chain F: 1-15; 326-347; 381-387.

GST-pull down assays

The C-terminal region of Gal4p (aa 768-881) was amplified and cloned into pGEX4T-1 vector using the BamHI/SalI restriction enzyme sites. This construct was transformed into BL21(DE3)-RIPL cells and expressed using standard procedures. The lysate was loaded onto glutathione agarose beads (SIGMA) and eluted with reduced glutathione. The eluted protein was further purified using a MonoQ column followed by gel filtration using a Superdex200 column. Free GST was also expressed using the pGex4T-1 vector and purified in a similar fashion. Concentrated proteins were aliquoted and stored at -70˚C until further use.

Gal80p and Gal80p-mutants were cloned into pET28a using the NdeI/SalI restriction enzyme sites and expressed as N-terminal $(His)_6$-tagged protein. These plasmids were

in vitro translated and ^{35}S-methionine-labeled using the TnT T7 rabbit reticulocyte system (Promega).

For the GST pulldowns assays, 300ng of GST, GST-Gal4p(768-881) or 600ng of GST-Gal3p was bound to 20µl slurry of glutathione sepharose beads (GE Healthcare) in the presence of 20mM Tris (pH 8.0), 0.2M KCl, 1mM EDTA, 0.02% NP-40, 10% glycerol and β-mercaptoethanol was added to a final concentration of 5mM. 8µl of *in vitro* translated Gal80p or Gal80p-mutants were added to the beads to a total volume of 250µl, in the presence or absence of NAD, NADH, NADP or NADPH (SIGMA) and incubated for 2hrs at 4˚C. Varying concentrations of the dinucleotide co-factor were added to the binding and wash buffer and maintained throughout the experiment. After three washes at 15min intervals, 60µl of SDS-PAGE loading buffer was added to the beads and boiled. 40µl of this sample was subjected to SDS-PAGE, dried and exposed on the Phosphor Imager (Fujifilm FLA-5100). Quantification was done with ImageJ (*16*). GST-Gal4p(842-875) was also tested and shows the same behavior as GST-Gal4p(768-881).

Kinetic analysis of *GAL1* induction

Strains were constructed in which the Gal80 protein (wild-type or mutant) was FLAG-tagged at its C-terminus and expressed from its own promoter at its natural locus (see Table S4). Cells were cultured in SC medium with 2% raffinose as carbon source at 30 ºC. Overnight cultures were diluted with fresh medium to an OD_{600} density of 0.2 to 0.3 and grown until OD_{600} 0.6~0.8. Galactose was added to a final concentration of 2% for *GAL* gene induction. Cells were collected at indicated times by centrifugation at 4ºC.

RNA was extracted from the cells using RiboPure-Yeast kit (Ambion) and converted to cDNA by Superscript II Reverse Transcriptase (Invitrogen). The expression levels of *GAL1* and *PMA1* in cDNA were evaluated by quantitative PCR with the LightCycler 480 system (Roche) using the following primers (5′ CGAAAAGTGCCCGAGCATAA 3′ and 5′ CAGCTAAAGCAACGGCACAA 3′ for *GAL1*; 5′ CTATTATTGATGCTTTGAAG ACCTCCAG 3′ and 5′ TGCCCAAAAT AATAGACATACCCCATAA 3′ for *PMA1*). For each time point, RNA levels were normalized to that found for uninduced wild type Gal80 and to PMA1 RNA. All experiments were performed in triplicate. Data are shown as mean and error bars indicate +/- standard deviations in Fig. 3. The t-test was used to determine whether differences between two samples are significant, *i.e.*, two samples are significantly different when $P<0.05$. Table S5 shows P values between wild type and mutant proteins.

Westerns

Levels of Gal80 protein, wild type or point mutants, were determined by western blotting of yeast cell extracts prepared as described previously (*17*). Proteins were transferred to PVDF membrane and blotted with anti-FLAG antibody to detect Gal80p and with anti-tubulin antibody (Sigma) as a loading control.

Tables

Table S1. Data collection statistics

Crystal	Native	Ta_6Br_{14}	Se (peak)	apo-form	NAD-soak
	←-------- --------Gal80-S2:P20 ----------→			←--------- Gal80-^{S0}-P21 ----------→	
X-ray source	X-25, NSLS	19ID, APS	X25-NSLS	X25-NSLS	X29-NSLS
Unit cell parameters	a=495.320Å	a=496.53Å	a=494.617Å	a=87.087Å	a=88.071Å
	b=84.862Å	b=85.434Å	b=85.229Å	b=103.947Å	b=103.431Å
	c=66.460Å	c=67.854Å	c=68.055Å	c=106.179Å	c=106.880Å
	β=98.90°	β=99.09°	β=98.093°		
Space group	C2	C2	C2	$P2_12_12$	$P2_12_12$
Overall mosaicity	0.5°	0.93°	0.604°	0.287°	0.716°
Wavelength(Å)	1.1	1.2519 (high energy remote)	0.9792	1.1	1.1
Resolution range (Å) (high resolution shell)	50-2.85 (2.95-2.85)	50-3.55 (3.68-3.55)	50-3.45 (3.57-3.45)	50-2.10 (2.18-2.10)	50-2.70 (2.80-2.70)
Total number of Reflections	1125473	430045	728294	1258846	1174596
Unique reflections	54557	30714	35649	57002	27466
Average I/σI	13.2 (2.11)	15.07 (3.63)	11.28 (2.06)	31.6 (2.06)	19.08 (1.87)
Completeness(%)	94.2(83.0)	90.9(91.9)	93.7(82.3)	99.9(99.8)	99.5(95.6)
Average Redundancy	2.3 (1.4)	4.9 (3.2)	2.9 (1.9)	9.6 (7.8)	6.5 (4.1)
R_{merge}(%)	7.6 (37.2)	10.5 (32.8)	8.1 (39.8)	7.9 (76.7)	9.1 (48.2)

Table S2. MIRAS phasing statistics for Gal80S2-P20

	Native2 + Ta_6Br_{14} (HER)	Native + Ta_6Br_{14} (HER) + Se(Peak)
	SIR(AS)	MIR(AS)
Number of sites	11	11+40
Resolution range used for Phasing	20 – 5.0Å	20-3.75 Å
Phasing power (acentric/centric)††	1.611/1.189	0.21/0.62
Rcullis (acentric/centric) ‡‡	0.59/0.69	0.93/0.92
Rcullis (anomalous)	0.593	0.83
Mean Figure of merit (f.o.m)¶ (MIRAS/ after Solomon)	0.49	0.309/0.71
Figure of merit (following density modification and phase extension)	0.74	
Resolution range (Å)	50-2.85	

[+]Fractional cell coordinates.
[§]Occupancy and anomalous occupancy are on arbitrary scales.
¶f.o.m. = $|F(hkl)_{best}|/|F(hkl)|$, with $F(hkl)_{best} = \sum_\alpha P(\alpha)F_{hkl}(\alpha)/\sum_\alpha P(\alpha)$
[++]Phasing power = r.m.s.($|F_H|/E$), where E is the residual lack of closure.
[‡‡]$R_{cullis} = \sum hkl \mid |F_{PH} \pm F_P| - |F_{H(calc)}| / \sum hkl \mid |F_{PH} - F_H|$

Table S3. Refinement Statistics

Model	Gal80^{S0}-P21-NAD	Gal80^{S0}	Gal80^{S2}
Resolution range (Å)	50-2.70	50-2.10	50-2.85
High resolution bin	(2.77-2.70)	(2.15-2.10)	2.93-2.85
Total number of reflections used	25891	54003	49054
R_{work} (%)[a]	23.5 (29.2)	23.9 (27.5)	24.8 (33.2)[b]
R_{free} (%)	27.8 (36.4)	27.4 (34.0)	31.4 (43.0)
Reflections used in the free set	1395	2867	5498
Number of molecules in the asymmetric unit	2	2	6
Number of protein atoms, peptide	5962, 70	6102	18487
Number of NAD atoms	88	-	-
Number of water molecules	23	232	17
R.M.S. bonds(Å), angles(°)	0.007, 1.05	0.007, 0.97	0.008, 1.08
Ramachandran plot (%)[c, d]			
Gal80-A	92.4/7.6/0/0	92.7/7.3/0/0	87.2/11.7/0.9/0.3
Gal80-B	90.4/9.3/0.3/0	93.3/6.7/0/0	86.0/13.1/0.6/0.3
Gal80-C			86.0/12.9/1.2/0
Gal80-D			88.3/10.5/0.9/0.3
Gal80-E			84.7/14.7/0.6/0
Gal80-F			83.8/14.7/1.5/0

[a] $R = \sum | | F_{obs} | - | F_{calc} | | / \sum | F_{obs} |$.

[b] The number in parentheses refers to the R-factor in the highest resolution bin

[c] Most favored / additionally allowed / generously allowed / disallowed regions of the Ramachandran plot, as calculated by Procheck.

[d] Arg142 is an outlier in monomers A & B of the Gal80p^{S2}:P20 however its side chain makes hydrogen bonds to the backbone and side chain oxygens of Ser110. Tyr 433 is an outlier in monomer D, however, the side chain of Arg410 makes a hydrogen bond to the backbone oxygen of Tyr433 as well as a NH-π interaction.

Table S4. Mutant strains

Strain	Genotype
BY4741	*MAT*a *his3Δ1 leu2Δ0 met15Δ0 ura3Δ0*
YYY17	BY4741, *GAL80::FLAG::S.p.his5*$^{+}$
YYY24	BY4741, *gal80-K29E::FLAG::S.p.his5*$^{+}$
YYY25	BY4741, *gal80-W31A::FLAG::S.p.his5*$^{+}$
YYY26	BY4741, *gal80-H36F::FLAG::S.p.his5*$^{+}$
YYY27	BY4741, *gal80-H99A::FLAG::S.p.his5*$^{+}$

Table S5. P-values between wild-type and mutant proteins at 5 and 15 minutes post induction. Red indicates significant differences (P<0.05).

	5 min	15 min
K29E	0.01894	0.04583
W31A	0.02634	0.30485
H36F	0.00011	0.00274
H99A	0.77489	0.97714
N230R	0.00001	0.00345

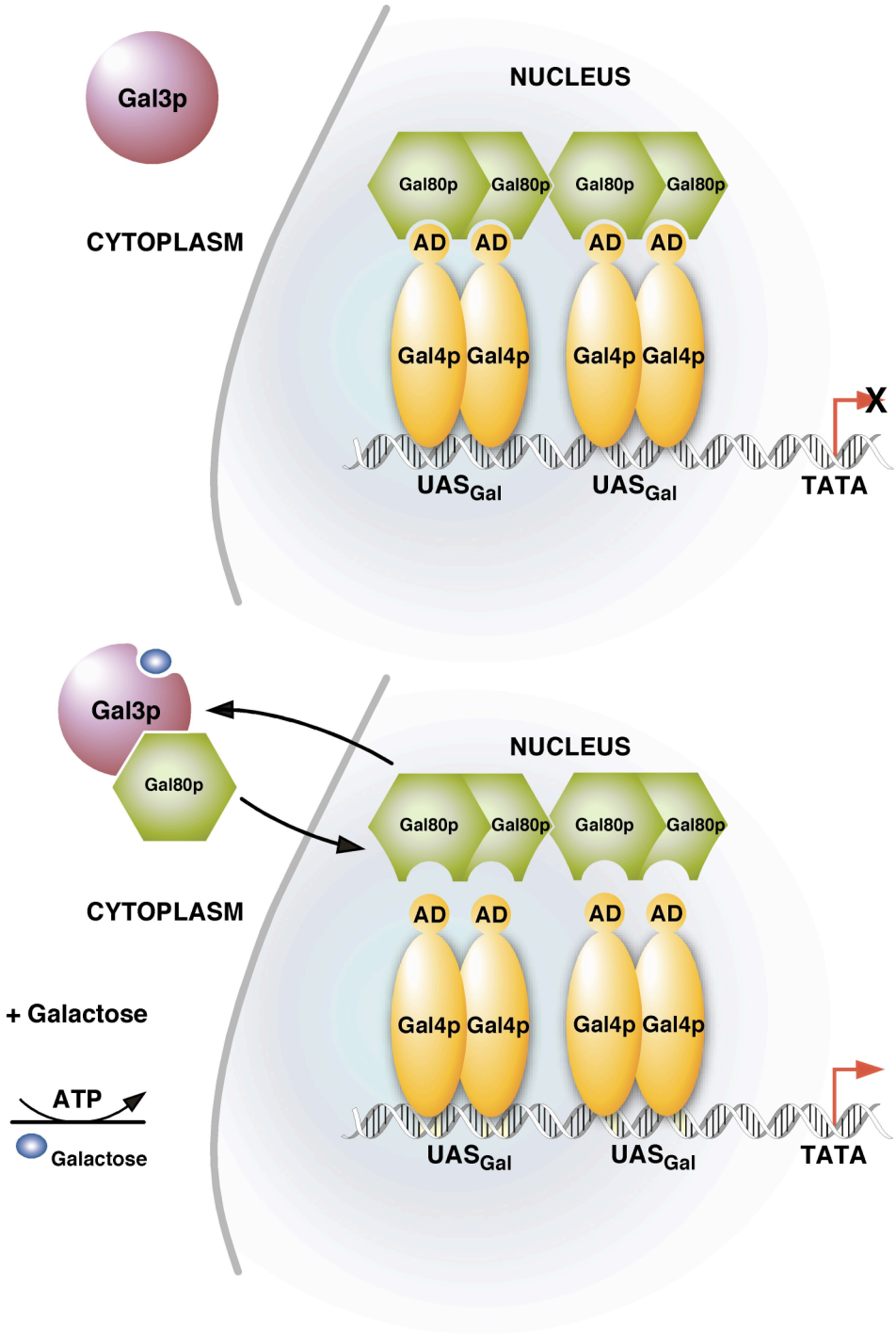

Figure S1. Current model of the yeast *GAL* transcriptional regulatory system. In non-inducing conditions, Gal4p binds as a dimer to each UAS$_{GAL}$ DNA-binding site. The *GAL1* promoter has four such UAS$_{GAL}$ elements. The negative regulator, Gal80p, binds to the Gal4p activation domain blocking transcription. Gal80p dimer-dimer interactions on adjacent UAS$_{GAL}$ elements effect synergistic control (see text). Upon induction, galactose binds to Gal3p with ATP, relieving repression by Gal80p and triggering activation of the *GAL* genes. Gal3p does not enter the nucleus but binds and sequesters Gal80p in the cytoplasm.

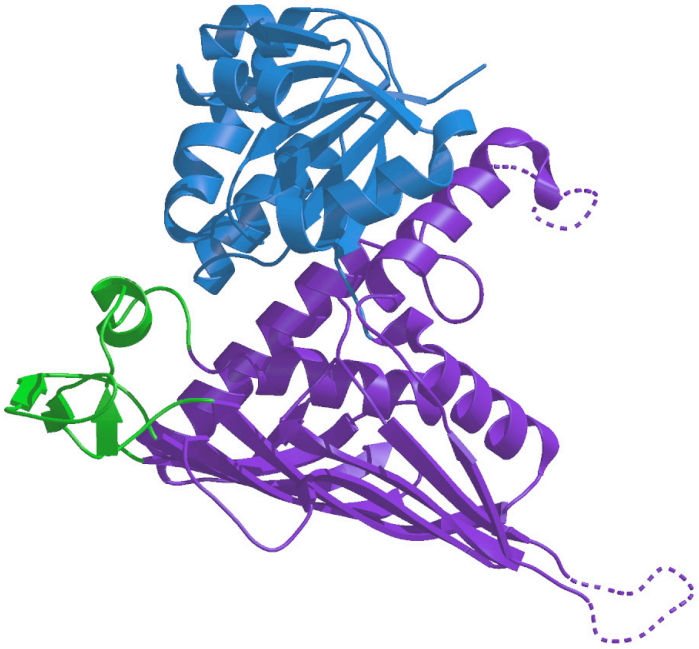

Figure S2. The monomer of Gal80p is comprised of three domains. The N-terminal domain (in blue) consists of a Rossman fold, the C-terminal domain (purple) with a prominent β-sheet forms the dimer interface, and a third domain (green) extends from the C-terminal domain toward the cleft. Disordered regions are shown as a dashed coil.

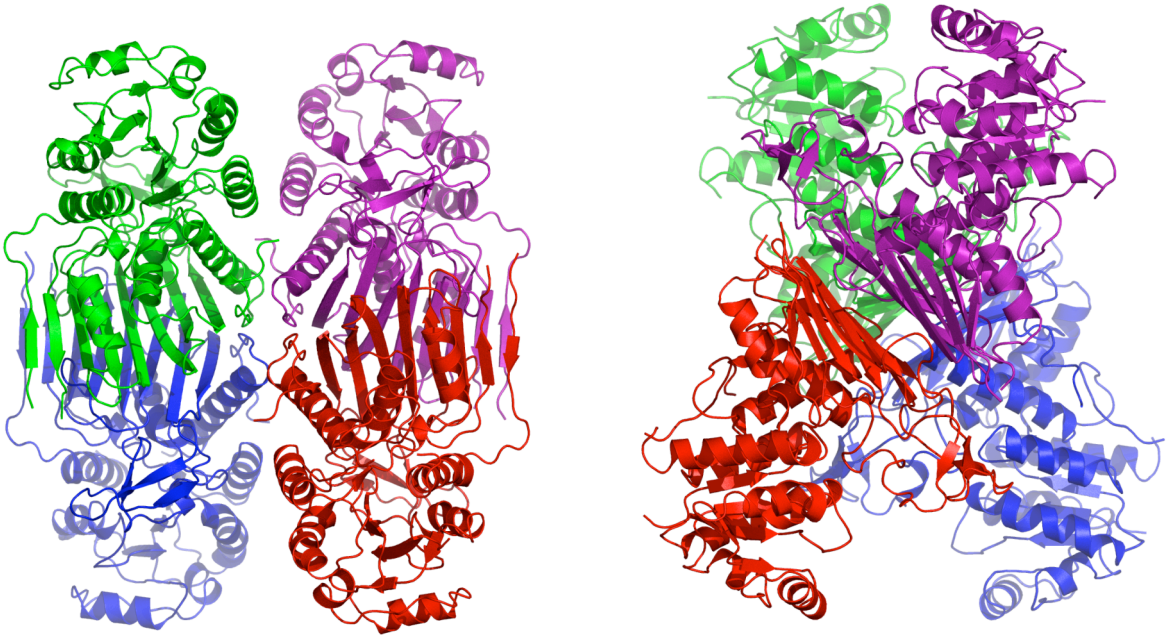

Figure S3. Two views of the tetrameric organization of Gal80p^{S2}. Two of the three dimers in the asymmetric unit are shown. The third dimer forms a similar tetramer with a crystallographically related dimer.

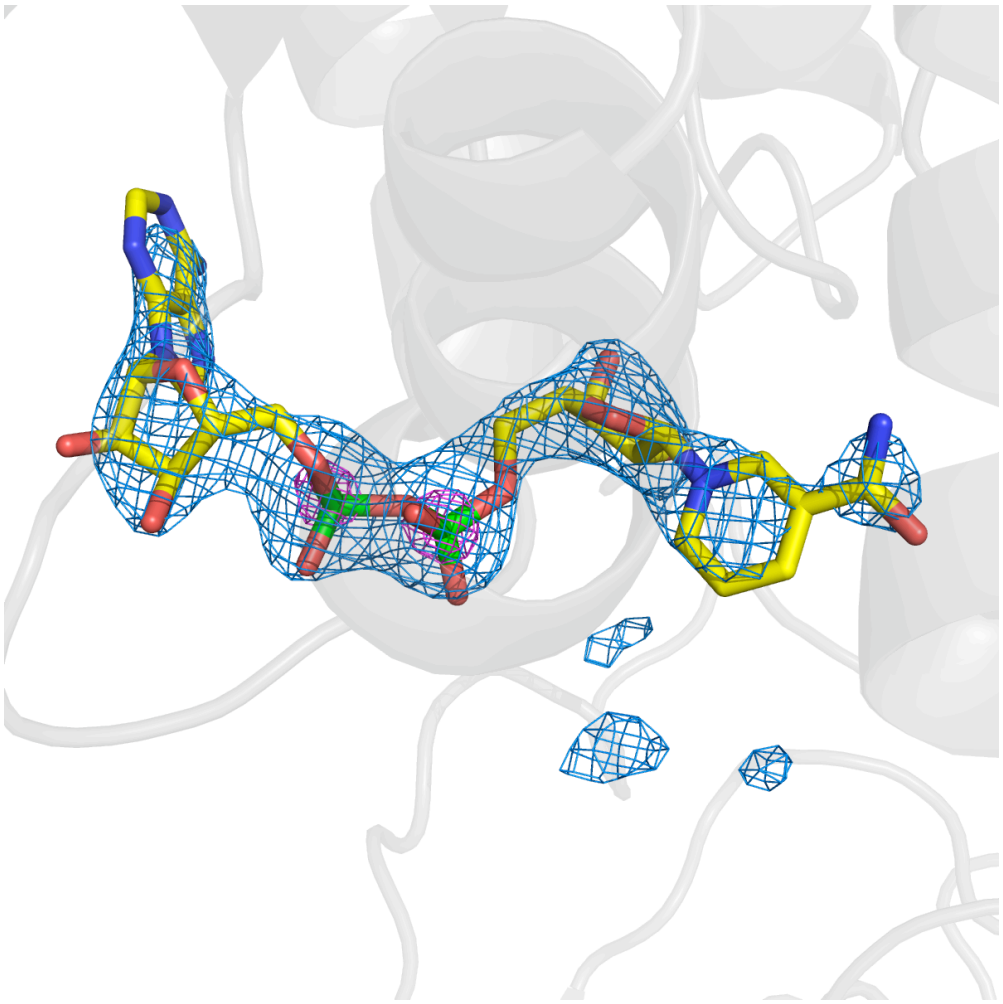

Figure S4. Difference electron density for the NAD soaked Gal80p^{S0}:P21 crystal, shows a clearly bound NAD molecule. The density is contoured in blue at 4σ and magenta at 9σ and was calculated prior to including NAD in the refinement. This feature is observed in both monomers of Gal80p^{S0}:P21 crystals. The refined structure of the NAD is superposed on the electron density.

(A)

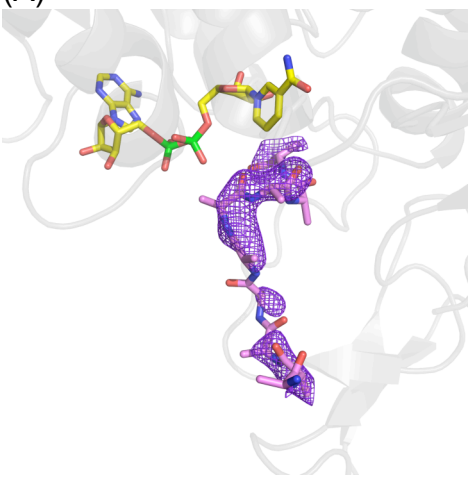

(C)

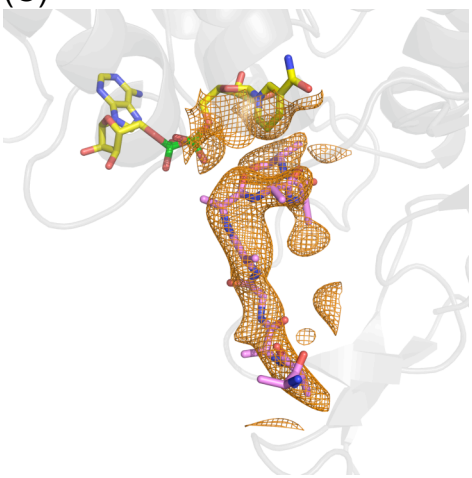

(B)

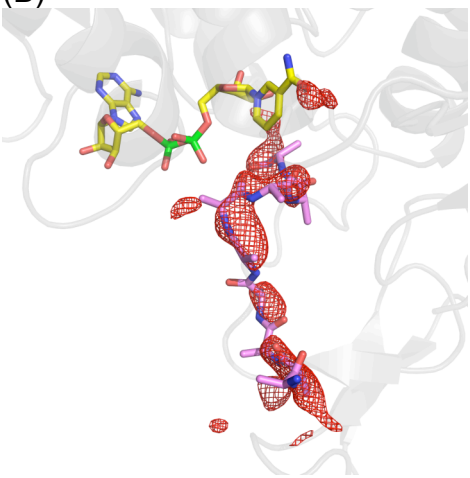

Figure S5. (A) Difference density for the peptide fragment contoured at 2.5σ, prior to inclusion of the peptide in the refinement but after inclusion of NAD. **(B)** Omit map contoured at 2.5σ, where the peptide was omitted, the rest of the coordinates randomly perturbed and subjected to refinement until convergence, using REFMAC. **(C)** 2Fo-Fc electron density contoured at 1.0σ around the peptide fragment. The final refined peptide fragment is superposed in all the figures.

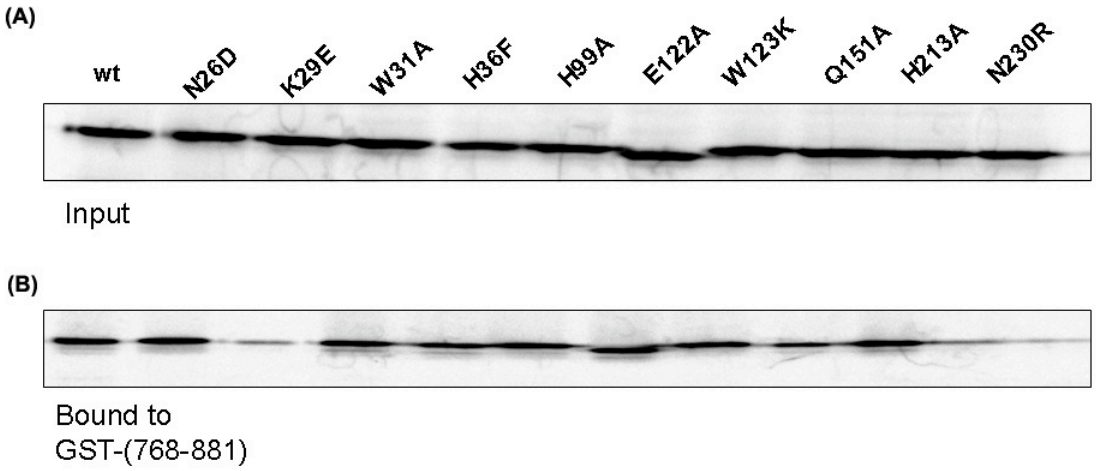

Figure S6. (A) Similar expression level of the wild-type Gal80p and mutants. Proteins were expressed as ^{35}S-labeled proteins in the TnT rabbit reticulocyte. 0.25 µl of the expressed protein, corresponding to 1% of protein used in the GST pull-down experiments, was loaded onto an SDS gel and subjected to electrophoresis. (B) 9 µl of ^{35}S-labeled protein, wild type or mutant, was bound to 300 ng of GST-Gal4p(768-881) bound to glutathione agarose beads. After 1 hour incubation, the beads were washed three times in the same buffer used for the GST pull-down experiments, but with no dinucleotides present. The gel shows varying levels of binding to Gal4p-AD. The faster migration of the Gal80p E122A mutant is reproducible and is not due to a deletion in the protein (see also Figure S7).

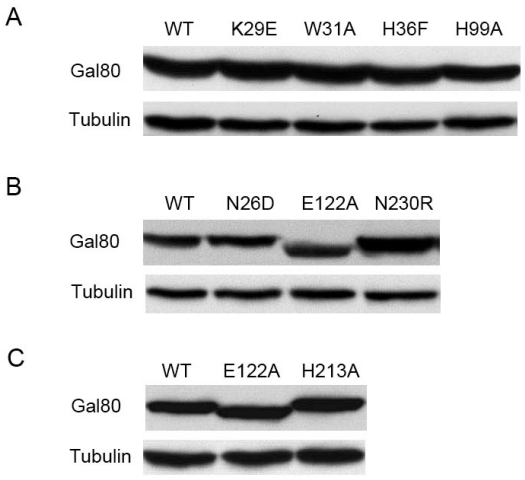

Figure S7. Expression of wild type (WT) Gal80p protein and various point mutants. The proteins were C-terminally tagged with the FLAG epitope and expressed from the endogenous *GAL80* locus. Yeast extracts were probed with an anti-FLAG antibody and with an anti-tubulin antibody as a loading control. The faster migration of the Gal80p E122A mutant is reproducible and is not due to a deletion in the protein (see also Figure S6).

References

1. Y. Han, T. Kodadek, *J. Biol. Chem.* **275**, 14979 (2000).
2. L. Holm, C. Sander, *J. Mol. Biol.* **233**, 123 (1993).
3. R. L. Kingston, R. K. Scopes, E. N. Baker, *Structure* **4**, 1413 (1996).
4. J. B. Thoden, C. A. Sellick, R. J. Reece, H. M. Holden, *J. Biol. Chem.* **282**, 1534 (2007).
5. R. Marmorstein, M. Carey, M. Ptashne, S. C. Harrison, *Nature* **356**, 408 (1992).
6. T. Pan, J. E. Coleman, *Proc. Natl. Acad. Sci., USA* **86**, 3145 (1989).
7. T. Pan, J. E. Coleman, *Biochemistry* **29**, 2023 (1990).
8. K. Melcher, H. E. Xu, *EMBO J.* **20**, 841 (2001).
9. M. Ptashne, *A Genetic Switch* (Blackwell Scientific Publications & Cell Press, Cambridge, MA, 1986), pp. 128.
10. T. R. Schneider, G. M. Sheldrick, *Acta Crystallogr. D Biol. Crystallogr.* **58**, 1772 (2002).
11. C. Vonrhein, E. Blanc, P. Roversi, G. Bricogne, *Methods Mol. Biol.* **364**, 215 (2006).
12. J. P. Abrahams, A. G. Leslie, *Acta Crystallogr. D Biol. Crystallogr.* **52**, 30 (1996).
13. T. A. Jones, M. Kjeldgaard, *Methods in Enzymol.* **277**, 173 (1997).
14. A. J. McCoy *et al.*, *J. Appl. Cryst.* **40**, 658 (2007).
15. M. D. Winn, M. N. Isupov, G. N. Murshudov, *Acta Crystallogr. D Biol. Crystallogr.* **57**, 122 (2001).
16. M. D. Abramoff, P. J. Magelhaes, S. J. Ram, *Biophotonics International* **11**, 36 (2004).
17. T. Krishnamoorthy *et al.*, *Genes Dev* **20**, 2580 (2006).